BOLD Signal in the Presence of Task-Correlated Respiratory Events

Sam Zorowitz

Abstract Please provide an abstract of no more than 150 words. Your abstract should explain the main contributions of your article, and should not contain any material that is not included in the main text.

Introduction

The goal of functional magnetic resonance imaging (fMRI) is to measure changes in the blood oxygenation level dependent (BOLD) signal as a proxy for induced changes in neural activity. This goal is stymied, however, by the fact that the signal changes of interest are often orders of magnitude smaller than artifactual noise caused by scanner noise, subject motion, and respiration (Huettel et al., 2004; Caballero-Gaudes and Reynolds, 2017).

Respiratory artifact is mediated largely by changes in arterial levels of carbon dioxide. Hypercapnic events (e.g. breath-holding) induce dramatic decreases in the BOLD signal (Kastrup et al., 1999a, 1999b). Even subtle changes in breathing depth and rate, which occur naturally (Van den Aardweg and Karemaker, 2002; Birn et al., 2006), can lead to significant changes in BOLD signal (Wise et al., 2004; Birn et al., 2006; Bianciardi et al., 2009a, 2009b). Despite this, cardiac and respiratory fluctuations account for less than 10% of the noise on average over the whole brain (Shmueli et al., 2007; Bianciardi et al., 2009a, 2009b). As such, many neuroimaging studies ignore respiratory noise when analyzing task-based fMRI data.

In recent years, there has been a renewed interest in respiratory artifact in task-based fMRI for two reasons. The first is a growing awareness of task-correlated changes in breathing rate, wherein respiratory artifact is time-locked to some event of interest.(Napadow et al., 2008; Birn et al., 2009; Huijbers et al., 2014) Task-correlated respiratory artifact may mask effects of interest or yield spurious findings if uncorrected for. The second is a growing realization that an especially pernicious form of motion artifact is likely caused by sudden changes in respiration (e.g. sharp inhale/exhale).(Power et al., 2018) This has prompted new research into novel methods for de-noising contaminated data,(Kundu et al., 2013; Power et al., 2018) and also suggests a need for improved coaching of subjects participating in fMRI studies.

For the NEU502b fMRI project, the class will investigate the effects of respiratory artifact on task-based fMRI data. Specifically, we will investigate the extent to which states of hypercapnia (excess CO2) and hypocapnia (diminished CO2) mask BOLD activity measured during the classic visual checkerboard paradigm. Hypercapnic and hypocapnic states will be induced using the breath-hold and controlled breathings tasks, respectively.(Birn et al., 2009; Bright et al., 2009) (If time permits, a novel sharp-inhale paradigm will also be scanned.) A list of possible analyses are proposed below.

Results

Visual Stimulation

To measure the effects of task-correlated respiratory artifact on the BOLD signal, a baseline must first be established. Participants viewed six blocks of flashing visual checkerboard each lasting 20s. Voxel-wise whole-brain GLM regression was performed using an idealized response to the checkerboard. Visual stimulation with the checkerboard yielded robust activation in bilateral visual cortex of both participants (Figure 1a/b). For each participant and hemisphere, a mask comprised of voxels belonging to the largest contiguous activation cluster was created. The average timecourse of voxels within each mask is presented is also presented (Figure

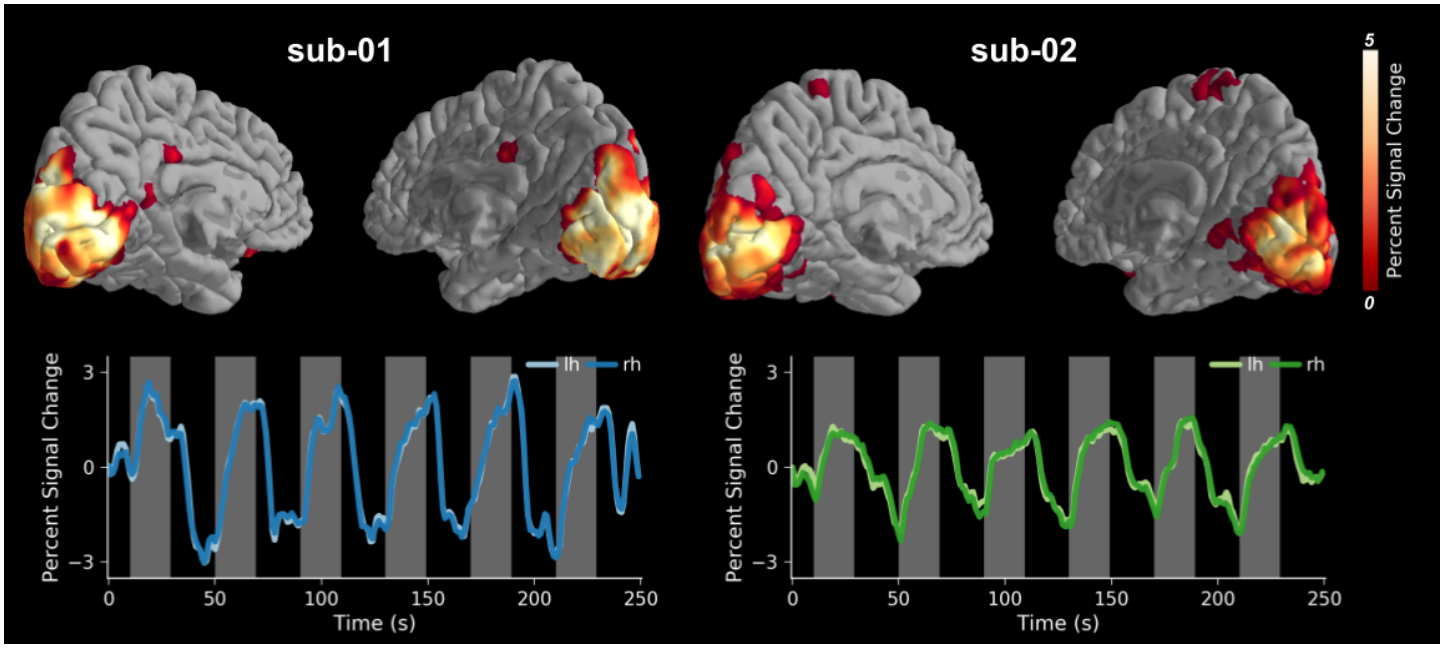

Figure 1. BOLD Change to Visual Stimulation

1c). On average, significantly activated voxels showed a 3.1 (sd=2.23) and 3.1 (sd=1.66) percent signal change in the left and right visual cortex for participant 1; significantly activated voxels showed a 1.69 (sd=1.26) and 1.75 (sd=1.03) percent signal change in the left and right visual cortex for participant 2.

Next, the effects of task-correlated respiratory artifact was measured in the presence of a hypercapniac and hypocapniac (breath-holding and hyperventilation, respectively). When the response to visual stimulation was measured without accounting for breath-holding, significant BOLD activation was detected across the cortex (Figure 2a / S1a). Conversely, when the response to visual stimulation was measured without accounting for hyperventilation, significant BOLD deactivation was detected across the cortex (Figure 2b / S1b). These results show a significant reduction in detection power (defined as accuracy in correctly estimating BOLD changes where there is, not not where there isn't) in the presence of uncontrolled respiratory-artifact.

Task-Correlated Respiratory Artifact

Averaged whole-brain responses to respiratory events, with their corresponding respiratory recordings, are presented in Figure 3. Consistent with previous reports, the BOLD response to a hypercapniac event (breath-holding) is characterized by an initial reduction in percent signal change followed by robust, prolonged increase peaking between 25s to 30s, and decreasing thereafter. Conversely, the BOLD response to a hypocapniac event (hyperventilation) is nearly the exact opposite: an initial increase in percent signal change followed by robust, prolonged decrease peaking around 25s and recovering slowly thereafter.

Next, testing for estimation power. Using the visual cortex maps defined above, we extracted the average percent signal change to visual stimulation in both the breath-holding and hyperventilation conditions. Collapsing across hemispheres, pairwise contrasts were computed to estimate the effects of respiratory events on visual stimulation. Except in one instance, the estimated BOLD response in visual cortex to visual stimulation was significantly reduced in the presence of both types of respiratory events (sub-01 control vs. breath-holding: $F = 0.04$, $p = 0.848$; sub-01 control vs. hyperventilation: $F = 38.19$, $p < 0.001$; sub-02 control vs. breath-holding: $F = 24.45$, $p < 0.001$; sub-02 control vs. hyperventilation: $F = 20.94$, $p < 0.001$).

NOTE ANATOMICAL VARIABILITY IN BOLD CHANGE

In summary, task-correlated respiratory artifact, when uncontrolled for, can result in substantially reduced detection power (i.e. increase in false positives) and estimation power (i.e. significant reduction of true effects).

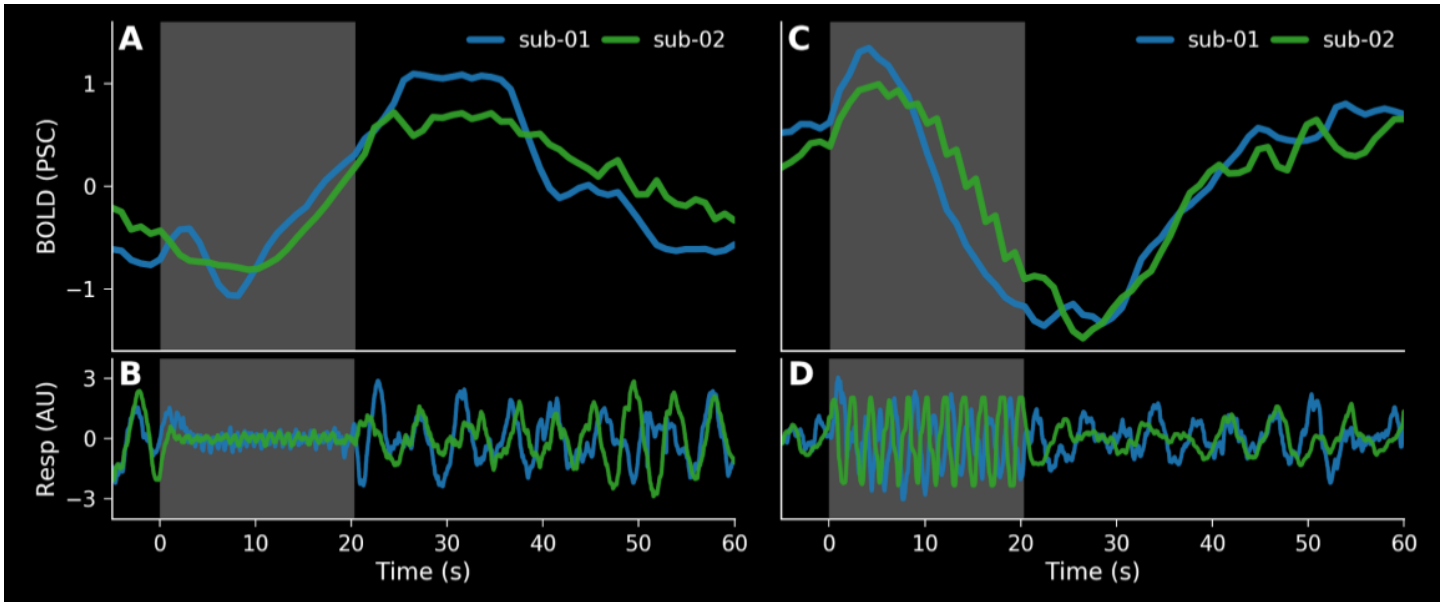

Figure 2. Respiratory Event Waveform

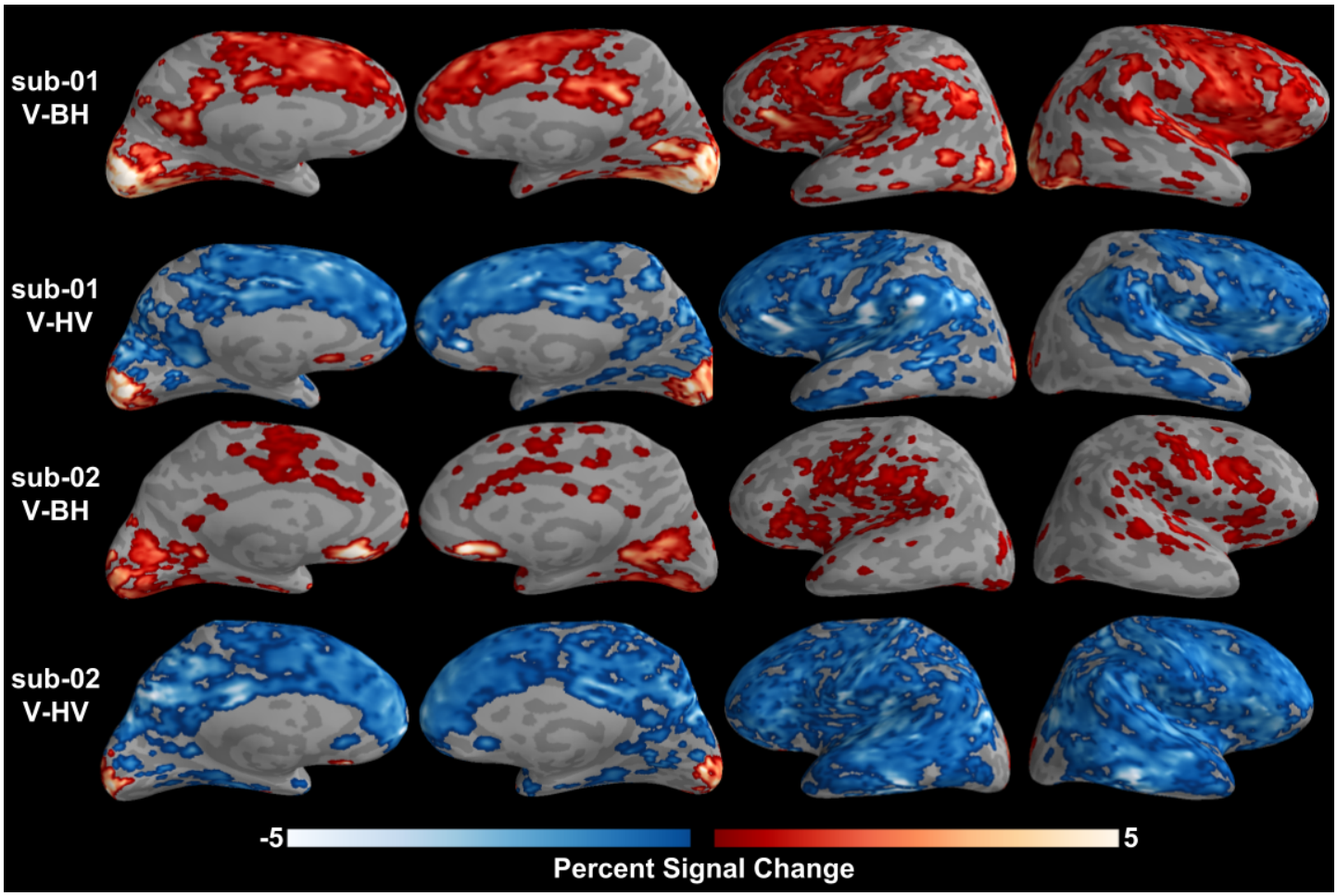

Figure 3. Task-correlated respiratory artifact

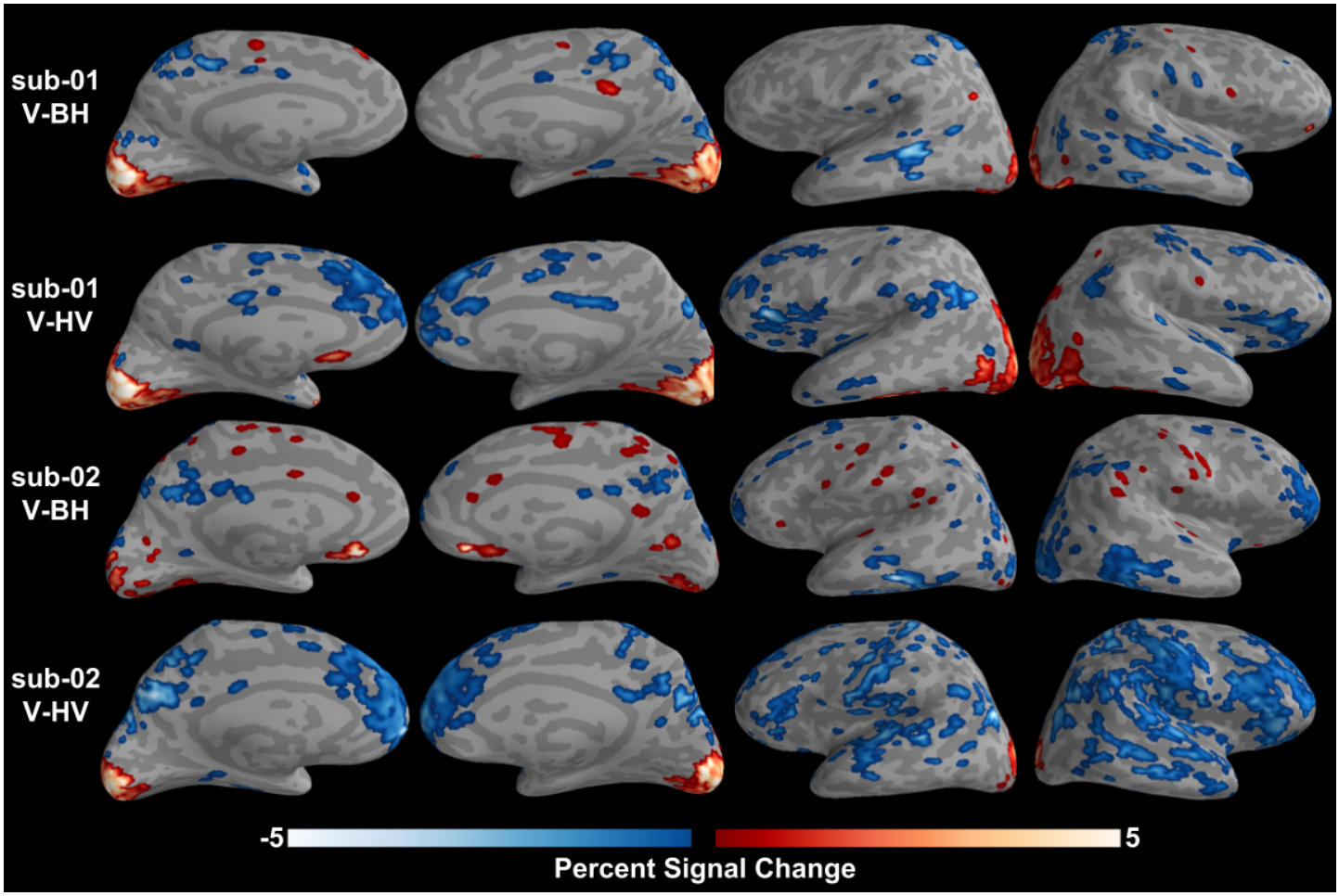

Figure 4. Correcting for artifact with CompCor

Correcting for Task-Correlated Respiration

Discussion

Methods

Participants

All experimental procedures were approved by the NEU502b course instructors. Two participants (both female, age 25) volunteered to participate in this experiment as part of a course on cognitive neuroscience methods. Both participants reported being right-handed and without a current or past diagnosis of a psychiatric or neurological disorder.

Task Paradigms

Visual Stimulation The visual localizer task was used to detect BOLD response visual cortex. To evoke a BOLD response, participants viewed a rotating and flashing black-and-white checkerboard stimulus. Each stimulus lasted 20 s followed by 20 s of fixation. The checkerboard stimulus was presented six total times. The run lasted 250 s.

Breathhold The breathholding task was used to measure the physiological BOLD response to a hypercapniac event. Participants were instructed to hold their breath for 20 s, followed by a recovery period of 40 s. Participants completed six total trials of breathholding. The run lasted 370 s.

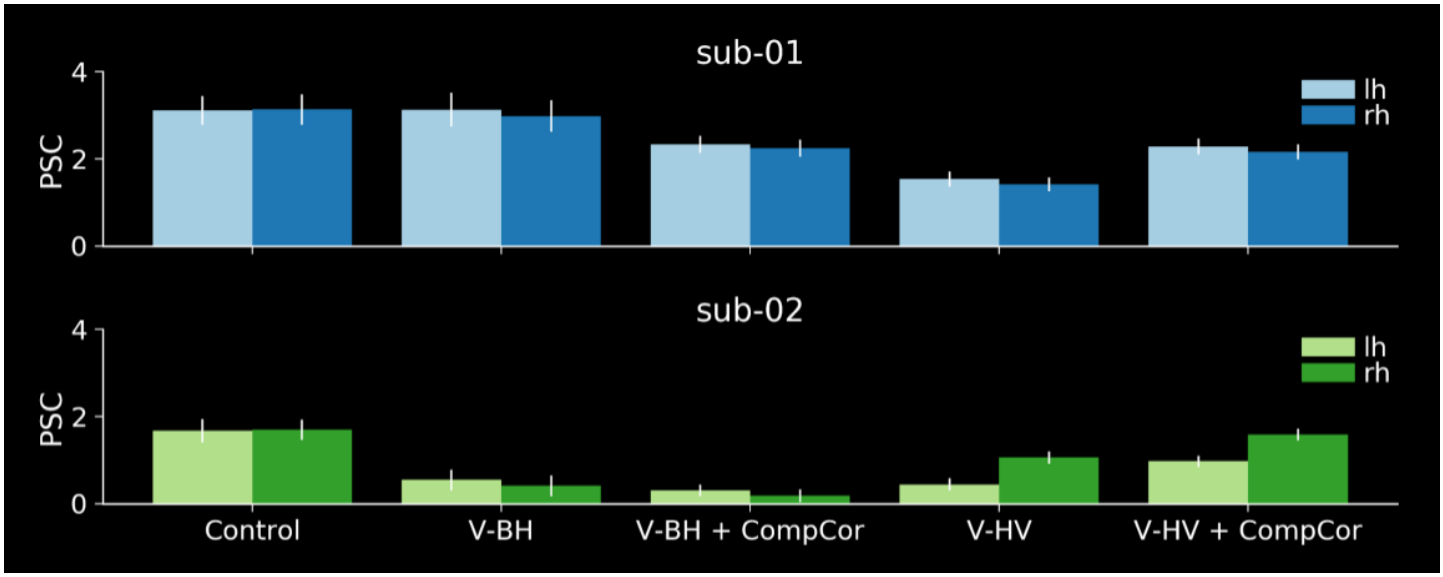

Figure 5. Respiratory Event Waveform

Hyperventilate The hyperventilation task was used to measure the physiological BOLD response to a hypocapniac event. Participants were coached rapidly inhale then exhale, with each action lasting 2 s. This was followed by a recovery period of 40 s. Participants completed six total trials of hyperventilation. The run lasted 370 s.

Visual Breathhold The visual-breathhold task was designed to measure the effects of a hypercapniac event on BOLD detection in visual cortex. Participants were again instructed to hold their breath for 20 s. After 10 s elapsed, the same checkerboard stimuli as above were presented for 20 s such that breathholding ended 10 s into the presentation of the visual stimulus. Blocks of breathholding and visual stimuli were separated by 30 s of fixation. The run lasted 370 s.

Visual Hyperventilate The visual-hyperventilation task was designed to measure the effects of a hypocapniac event on BOLD detection in visual cortex. Participants were again coached in rapid breathing for 20 s. After 10 s elapsed, the same checkerboard stimuli as above were presented for 20 s such that hyperventilation ended 10 s into the presentation of the visual stimulus. Blocks of hyperventilation and visual stimuli were separated by 30 s of fixation. The run lasted 370 s.

Visual stimuli were programmed in Python and Psychopy(Peirce, 2008) and were presented with a projector. Participants viewed the projection on a screen fixed at the back of the scanner bore, through a mirror fixed in front of the eyes.

Data Acquisition

Briefly, all images were acquired with a 64 channel head coil on a 3T Siemens Prisma. A T1-weighted MPRAGE image was acquired with TR=2530 ms, TE 3.31 ms, flip angle=7 deg, in-plane FOV=256 x 256 mm, 176 slices, 1.0 mm isotropic voxels. For advanced anatomical registration (see below), a T2-weighted image was acquired TR=3200 ms, TE=428 ms, flip angle=120 deg, in-plane FOV=256 × 256 mm, 72 slices, 1.0 mm isotropic voxels. Whole-brain EPI acquisitions were acquired with TR=1000 ms, TE=30 ms, flip angle=55 deg, in-plane FOV=192 × 192 mm, 56 slices, 3.0 mm isotropic voxels, with a multi-band acceleration factor of 4. One run of each task was acquired with anterior-to-posterior phase encoding. Prior to the collection of the EPI images, a fieldmap was acquired for the purposes of susceptibility distortion correction (see below) with TR=1000 ms, TE=3.47 ms, flip angle=120 deg, in-plane FOV=192 × 192 mm, 56 slices, 3.0 mm isotropic voxels.

To measure cardiac and respiratory signals, a pulse oximeter and respiratory bellows were fitted to participants prior to the scanning. The pulse and respiratory signals were recorded by the scanner host computer at a sampling rate of 200 Hz and 50 Hz, respectively. The recordings were aligned with the onset of the first sync pulse using a custom script.

Data Preprocessing

Results included in this manuscript come from preprocessing performed using FMRIPREP v1.0.8 (Esteban et al., 2018), a Nipype based tool (Gorgolewski et al., 2011, 2017). Each T1w (T1-weighted) volume was corrected for INU (intensity non-uniformity) using *N4BiasFieldCorrection* v2.1.0 (Tustison et al., 2010) and skull-stripped using *antsBrainExtraction.sh* v2.1.0 (using the OASIS template). Brain surfaces were reconstructed using *recon-all* from FreeSurfer v6.0.0 (Dale et al., 1999), and the brain mask estimated previously was refined with a custom variation of the method to reconcile ANTs-derived and FreeSurfer-derived segmentations of the cortical gray-matter of Mindboggle (Klein et al., 2017). Spatial normalization to the ICBM 152 Nonlinear Asymmetrical template version 2009c (Fonov et al., 2009) was performed through nonlinear registration with the *antsRegistration* tool of ANTs v2.1.0 (Avants et al., 2008), using brain-extracted versions of both T1w volume and template. Brain tissue segmentation of cerebrospinal fluid (CSF), white-matter (WM) and gray-matter (GM) was performed on the brain-extracted T1w using *fast* (FSL v5.0.9) (Zhang et al., 2001).

Functional data was motion corrected using *mcflirt* (FSL v5.0.9; Jenkinson et al., 2002). Slice timing was not performed in light of the task design and short repetition time. Distortion correction was performed using an implementation of the TOPUP technique (Andersson et al., 2003) using *3dQwarp* (AFNI v16.2.07; Cox, 1996). This was followed by co-registration to the corresponding T1w using boundary-based registration (Greve and Fischl, 2009) with 9 degrees of freedom, using *bbregister* (FreeSurfer v6.0.0). Motion correcting transformations, field distortion correcting warp, BOLD-to-T1w transformation and T1w-to-template (MNI) warp were concatenated and applied in a single step using *antsApplyTransforms* (ANTs v2.1.0) using Lanczos interpolation.

Physiological noise regressors were extracted applying CompCor (Behzadi et al., 2007). Principal components were estimated for the two CompCor variants: temporal (tCompCor) and anatomical (aCompCor). A mask to exclude signal with cortical origin was obtained by eroding the brain mask, ensuring it only contained subcortical structures. Six tCompCor components were then calculated including only the top 5% variable voxels within that subcortical mask. For aCompCor, six components were calculated within the intersection of the subcortical mask and the union of CSF and WM masks calculated in T1w space, after their projection to the native space of each functional run. Framewise displacement (Power et al., 2014) was calculated for each functional run using the implementation of Nipype.

Many internal operations of FMRIPREP use *Nilearn* (Abraham et al., 2014), principally within the BOLD-processing workflow. For more details of the pipeline see https://fmriprep.readthedocs.io/en/latest/workflows.html.

Image quality was assessed using MRIQC v0.10.4 (Esteban et al., 2017). Both anatomical and functional scans were visually inspected for artifacts and showed no apparent defects. For completeness, the QC reports, including carpet plots of the raw BOLD signal (Power, 2017), are included for inspection.

Data Analysis

Prior to regression analysis, all functional data were downsampled to the *fsaverage5* template brain (10242 vertices per hemisphere). This 10-fold reduction in mesh vertices is similar to applying spatial smoothing with FWHM of approximately 6 mm^2. To remove low frequency drift terms, functional data were also high-passed filtered at 100s using Nilearn.

Functional activation maps in response to the visual checkerboard stimulus were obtained by regressing each voxel time series against a boxcar function corresponding to the onset/offset times of the stimulus convolved with the canonical hemodynamic response function. In the first analysis (localizer), the ideal task response was modeled in the uncorrupted runs (run 1). In the second analysis, the ideal task response was modeled in the presence of task-correlated respiratory artifact (breath-holding and hyperventilation). In the third analysis, the ideal task response in the presence of task-correlated respiratory artifact and artifact regressors. In the fourth and final analysis, the ideal task response in the presence of task-correlated respiratory artifact and CompCor regressors.

For all analyses, additional nuisance regressors were included. These included the timeseries of motion, which were demeaned, linearly detrended, and orthogonalized prior to regression. We also include “motion scrubbers”, which remove volumes with high motion artifact (FD > 0.5) as previously recommended (Power et al., 2014; Siegel et al., 2014). To correct for temporal autocorrelation, the data and design matrices were prewhitened using a Tukey taper approach (Woolrich et al., 2001). Multiple comparisons corrections were implemented through permutation testing with 5000 null iterations and family-wise error correction at alpha = 0.05 (Winkler et al., 2014). Final results projected back onto native freesurfer brains for visualization.

References

Van den Aardweg JG, Karemaker JM. Influence of chemoreflexes on respiratory variability in healthy subjects. Am J Respir Crit Care Med. 2002 Apr; 165(8):1041–1047.

Abraham A, Pedregosa F, Eickenberg M, Gervais P, Mueller A, Kossaifi J, Gramfort A, Thirion B, Varoquaux G. Machine learning for neuroimaging with scikit-learn. Front Neuroinform. 2014 Feb; 8:14.

Andersson JLR, Skare S, Ashburner J. How to correct susceptibility distortions in spin-echo echo-planar images: application to diffusion tensor imaging. Neuroimage. 2003 Oct; 20(2):870–888.

Avants BB, Epstein CL, Grossman M, Gee JC. Symmetric diffeomorphic image registration with cross-correlation: evaluating automated labeling of elderly and neurodegenerative brain. Med Image Anal. 2008 Feb; 12(1):26–41.

Behzadi Y, Restom K, Liau J, Liu TT. A component based noise correction method (CompCor) for BOLD and perfusion based fMRI. Neuroimage. 2007 Aug; 37(1):90–101.

Bianciardi M, Fukunaga M, van Gelderen P, Horovitz SG, de Zwart JA, Duyn JH. Modulation of spontaneous fMRI activity in human visual cortex by behavioral state. Neuroimage. 2009 Mar; 45(1):160–168.

Bianciardi M, Fukunaga M, van Gelderen P, Horovitz SG, de Zwart JA, Shmueli K, Duyn JH. Sources of functional magnetic resonance imaging signal fluctuations in the human brain at rest: a 7 T study. Magn Reson Imaging. 2009 Oct; 27(8):1019–1029.

Birn RM, Diamond JB, Smith MA, Bandettini PA. Separating respiratory-variation-related fluctuations from neuronal-activity-related fluctuations in fMRI. Neuroimage. 2006 Jul; 31(4):1536–1548.

Birn RM, Murphy K, Handwerker DA, Bandettini PA. fMRI in the presence of task-correlated breathing variations. Neuroimage. 2009 Sep; 47(3):1092–1104.

Bright MG, Bulte DP, Jezzard P, Duyn JH. Characterization of regional heterogeneity in cerebrovascular reactivity dynamics using novel hypocapnia task and BOLD fMRI. Neuroimage. 2009; .

Caballero-Gaudes C, Reynolds RC. Methods for cleaning the BOLD fMRI signal. Neuroimage. 2017 Jul; 154:128–149.

Cox RW. AFNI: software for analysis and visualization of functional magnetic resonance neuroimages. Comput Biomed Res. 1996 Jun; 29(3):162–173.

Dale AM, Fischl B, Sereno MI. Cortical surface-based analysis. I. Segmentation and surface reconstruction. Neuroimage. 1999 Feb; 9(2):179–194.

Esteban O, Birman D, Schaer M, Koyejo OO, Poldrack RA, Gorgolewski KJ. MRIQC: Advancing the automatic prediction of image quality in MRI from unseen sites. PLoS One. 2017 Sep; 12(9):e0184661.

Esteban O, Blair R, Markiewicz CJ, Berleant SL, Moodie C, Ma F, Isik AI, Erramuzpe A, Kent JD, Goncalves M, DuPre E, Sitek KR, Poldrack RA, Gorgolewski KJ, poldracklab/fmriprep: 1.0.10; 2018.

Fonov VS, Evans AC, McKinstry RC, Almli CR, Collins DL. Unbiased nonlinear average age-appropriate brain templates from birth to adulthood. Neuroimage. 2009; 47:S102.

Gorgolewski K, Burns CD, Madison C, Clark D, Halchenko YO, Waskom ML, Ghosh SS. Nipype: a flexible, lightweight and extensible neuroimaging data processing framework in python. Front Neuroinform. 2011 Aug; 5:13.

Gorgolewski KJ, Esteban O, Ellis DG, Notter MP, Ziegler E, Johnson H, Hamalainen C, Yvernault B, Burns C, Manhães-Savio A, Jarecka D, Markiewicz CJ, Salo T, Clark D, Waskom M, Wong J, Modat M, Dewey BE, Clark MG, Dayan M, et al., Nipype: a flexible, lightweight and extensible neuroimaging data processing framework in Python. 0.13.1; 2017.

Greve DN, Fischl B. Accurate and robust brain image alignment using boundary-based registration. Neuroimage. 2009 Oct; 48(1):63–72.

Huettel SA, Song AW, McCarthy G, Others. Functional magnetic resonance imaging, vol. 1. Sinauer Associates Sunderland; 2004.

Huijbers W, Pennartz CMA, Beldzik E, Domagalik A, Vinck M, Hofman WF, Cabeza R, Daselaar SM. Respiration phase-locks to fast stimulus presentations: implications for the interpretation of posterior midline “deactivations”. Hum Brain Mapp. 2014 Sep; 35(9):4932–4943.

Jenkinson M, Bannister P, Brady M, Smith S. Improved optimization for the robust and accurate linear registration and motion correction of brain images. Neuroimage. 2002 Oct; 17(2):825–841.

Kastrup A, Krüger G, Glover GH, Neumann-Haefelin T, Moseley ME. Regional variability of cerebral blood oxygenation response to hypercapnia. Neuroimage. 1999 Dec; 10(6):675–681.

Kastrup A, Li TQ, Glover GH, Moseley ME. Cerebral blood flow-related signal changes during breath-holding. AJNR Am J Neuroradiol. 1999 Aug; 20(7):1233–1238.

Klein A, Ghosh SS, Bao FS, Giard J, Häme Y, Stavsky E, Lee N, Rossa B, Reuter M, Chaibub Neto E, Keshavan A. Mindboggling morphometry of human brains. PLoS Comput Biol. 2017 Feb; 13(2):e1005350.

Kundu P, Brenowitz ND, Voon V, Worbe Y, Vértes PE, Inati SJ, Saad ZS, Bandettini PA, Bullmore ET. Integrated strategy for improving functional connectivity mapping using multiecho fMRI. Proc Natl Acad Sci U S A. 2013 Oct; 110(40):16187–16192.

Napadow V, Dhond R, Conti G, Makris N, Brown EN, Barbieri R. Brain correlates of autonomic modulation: combining heart rate variability with fMRI. Neuroimage. 2008 Aug; 42(1):169–177.

Peirce JW. Generating Stimuli for Neuroscience Using PsychoPy. Front Neuroinform. 2008; 2:10.

Power JD. A simple but useful way to assess fMRI scan qualities. Neuroimage. 2017 Jul; 154:150–158.

Power JD, Mitra A, Laumann TO, Snyder AZ, Schlaggar BL, Petersen SE. Methods to detect, characterize, and remove motion artifact in resting state fMRI. Neuroimage. 2014 Jan; 84:320–341.

Power JD, Plitt M, Gotts SJ, Kundu P, Voon V, Bandettini PA, Martin A. Ridding fMRI data of motion-related influences: Removal of signals with distinct spatial and physical bases in multiecho data. Proc Natl Acad Sci U S A. 2018 Feb; 115(9):E2105–E2114.

Shmueli K, van Gelderen P, de Zwart JA, Horovitz SG, Fukunaga M, Jansma JM, Duyn JH. Low-frequency fluctuations in the cardiac rate as a source of variance in the resting-state fMRI BOLD signal. Neuroimage. 2007 Nov; 38(2):306–320.

Siegel JS, Power JD, Dubis JW, Vogel AC, Church JA, Schlaggar BL, Petersen SE. Statistical improvements in functional magnetic resonance imaging analyses produced by censoring high-motion data points. Hum Brain Mapp. 2014 May; 35(5):1981–1996.

Tustison NJ, Avants BB, Cook PA, Zheng Y, Egan A, Yushkevich PA, Gee JC. N4ITK: improved N3 bias correction. IEEE Trans Med Imaging. 2010 Jun; 29(6):1310–1320.

Winkler AM, Ridgway GR, Webster MA, Smith SM, Nichols TE. Permutation inference for the general linear model. Neuroimage. 2014 May; 92:381–397.

Wise RG, Ide K, Poulin MJ, Tracey I. Resting fluctuations in arterial carbon dioxide induce significant low frequency variations in BOLD signal. Neuroimage. 2004 Apr; 21(4):1652–1664.

Woolrich MW, Ripley BD, Brady M, Smith SM. Temporal autocorrelation in univariate linear modeling of FMRI data. Neuroimage. 2001 Dec; 14(6):1370–1386.

Zhang Y, Brady M, Smith S. Segmentation of brain MR images through a hidden Markov random field model and the expectation-maximization algorithm. IEEE Trans Med Imaging. 2001 Jan; 20(1):45–57.

Subject	Analysis	L PSC	R PSC	F-val	p-val
01	Viz	3.11 (0.33)	3.13 (0.35)		
	BH	3.13 (0.38)	2.98 (0.36)	0.04	0.848
	BH + CompCor	2.33 (0.20)	2.25 (0.20)	13.42	<0.001
	HV	1.53 (0.17)	1.41 (0.16)	38.19	<0.001
	HV + CompCor	2.28 (0.18)	2.16 (0.17)	17.29	<0.001
02	Viz	1.67 (0.27)	1.70 (0.23)		
	BH	0.54 (0.23)	0.41 (0.24)	24.45	<0.001
	BH + CompCor	0.30 (0.14)	0.18 (0.14)	73.14	<0.001
	HV	0.44 (0.14)	1.05 (0.14)	20.94	<0.001
	HV + CompCor	0.97 (0.13)	1.59 (0.13)	5.80	0.016

Table 1. Percent Signal Change in Visual Cortex Summary of estimated percent change of the BOLD signal in visual cortex across the tested models. Estimates are divided by subject (01/02) and hemisphere (left/right). The F statistic corresponding to the pairwise comparison of models to baseline (collapsing across hemisphere) is presented.